

GUIDANCE, NAVIGATION, AND CONTROL FOR NASA LUNAR PALLET LANDER

**Juan Orphee,¹ Mike Hannan,* Ellen Braden,² Evan Anzalone*, Naeem Ahmad*, Scott Craig*,
Nicholas Olson*, Jason Everett*, and Kyle Miller***

The NASA Lander Technology project is leading the development and integration of the Lunar Pallet Lander (LPL) concept. The objective is to demonstrate precision landing by delivering a payload to the lunar surface within 100 meters of a landing target. Potential landing sites are selected near the lunar pole where water may be present in permanently shadowed regions that could enable future in-situ resource utilization. The LPL is part of a sequence of missions aimed at maturing the necessary technologies, such as lunar precision landing sensors, that will enable the next generation of multi-ton lunar payloads and human landers. This paper provides an overview of the Mission Design, Guidance Navigation and Control (GNC) algorithms, and sensor suite. The results show the LPL simulated trajectory and landing precision performance under nominal and dispersed conditions. The landing precision simulation confirms the need to rely on high-accuracy navigation techniques and sensors such as Terrain Relative Navigation (TRN) and the Navigation Doppler Lidar (NDL), currently being developed for space applications. The results also demonstrate the ability of the guidance and control system to perform a soft lunar touchdown by combining thrust vector control during the solid rocket motor deceleration phase, and pulse engine control, for the liquid powered descent phase.

INTRODUCTION

In preparation for future robotic missions to the lunar surface, NASA has performed a number of concept studies to identify technology needs for upcoming lunar missions. These studies have spawned development efforts in advanced propulsion, navigation and landing, and various other lander subsystems. NASA has also independently developed and terrestrially flown lander test beds: Morpheus (led by NASA Johnson Space Center) and Mighty Eagle (led by NASA Marshall Space Flight Center).¹ Morpheus and Mighty Eagle demonstrated vehicle-level integration capabilities using different propulsion architectures, navigation and landing systems, ground and flight software, and avionics. The success of these efforts led to the establishment of an integrated, cross-agency lander community that now supports industry through several funded efforts under NASA's Advanced Exploration Systems (AES) Lander Technologies Project.

In one of the recent studies, the Lunar Pallet Lander (LPL) concept was introduced, as illustrated in Figure 1. The LPL is a lander capable of delivering a 300kg rover payload to the polar regions of the Moon. The rover would be able to perform science or be equipped with an In-Situ Resource Utilization (ISRU) demonstration payload. This lander was designed to minimize cost and schedule, with its mission terminating once the surface payload was delivered. While still emphasizing simplicity and affordability, this

¹ Aerospace Engineer, EV 42, NASA/Marshall Space Flight Center, Huntsville AL 35801

² Aerospace Engineer, EG511, NASA/Johnson Space Center, Houston, TX, 77058

lander design has been further evolved to investigate features potentially extensible to future human landers. Also, the LPL will provide power and communications to the payload from transit to lunar landing. Finally, lander is not intended to survive the lunar night.

This paper provides an overview of the LPL mission design, guidance, navigation, and control system. The paper is divided into five main sections. The first section, provides an overview of the mission design. Section two, defines the guidance, navigation and control algorithms. Section three, describes the multi-body dynamics generalized lander simulation tool. In addition, section four, describes the lander simulated performance during a lunar descent. Finally, section five summarizes the key findings and future work.

MISSION DESIGN

The LPL uses a combination of liquid propulsion and solid propulsion. The solid stage, composed of an ATK Star 48AV Solid Rocket Motor (SRM), is used for the braking burn, and it is jettisoned after SRM burnout. The liquid propulsion consists of twelve pulsed thrusters descent engines, 100 lbf each, three on each of the four corners of the vehicle, as shown in Figure 1 below. The liquid engines use a hypergolic bipropellant: a Monomethylhydrazine (MMH) as fuel, and 25% nitric oxide (MON25) as oxidizer.

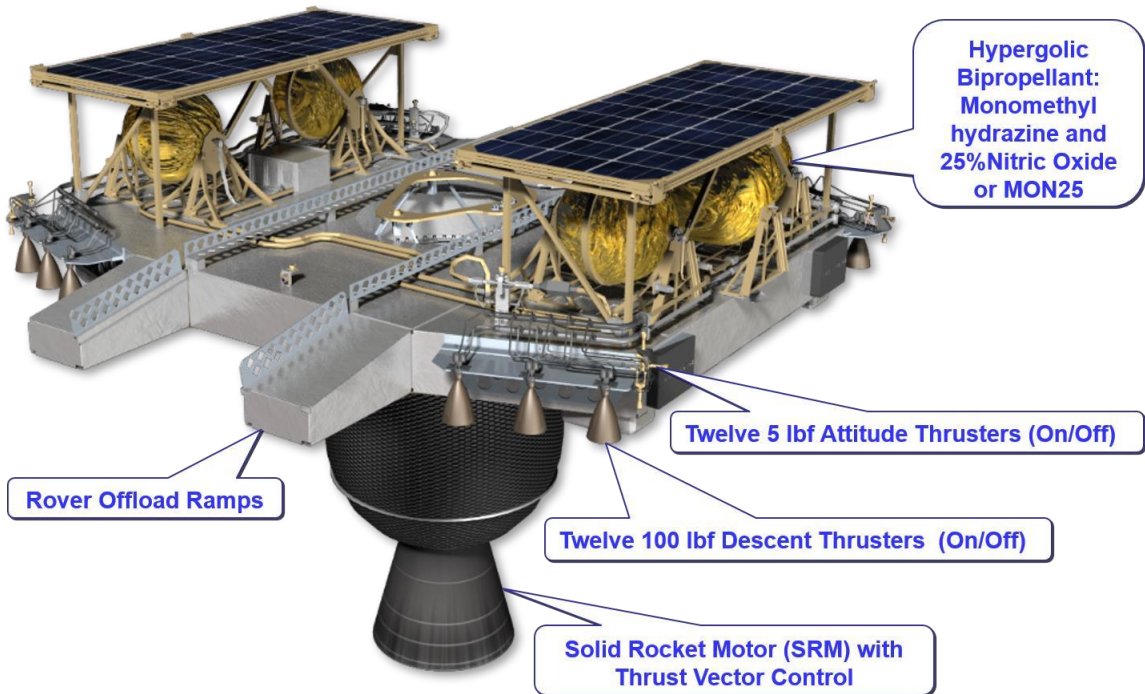


Figure 1. Lunar Pallet Lander Configuration, without Payload.

The LPL mission design assumes a ride on an Evolved Expendable Launch Vehicle (EELV) class vehicle. With the LPL as a primary payload, the mission design is greatly simplified, since the lander can fly into a direct descent to the lunar surface. Therefore, after the Trans Lunar Injection TLI burn, provided by the EELV, the LPL separates from the upper stage of the launch vehicle, as shown in the mission summary Figure 2. After system checkout and sun-pointing, the LPL will perform Trajectory Correction Maneuvers (TCMs) to “clean” any TLI insertion dispersions. The mission currently budgets a total of 25 m/s of deltaV

for all TCMs. After TLI, and any needed TCMs, the LPL cruises for approximately 4 days before initiating the breaking burn with the SRM. The LPL trajectory is optimized, to account for SRM performance variations due to solid propellant temperature, Figure 3, and navigation uncertainties during the SRM burn that could bias the trajectory as much as ± 6 km in crossrange and downrange. ^{2,3} After the solid burn is completed, a short coast of 30 seconds allows the vehicle to maneuver to its optimal liquid descent burn orientation. The final liquid burn is decomposed on three phases. The first phase uses Apollo's optimal guidance with a target at 200 meters above the lunar surface, and a descent velocity of 10m/s. ⁴ Then, the second phase is a vertical descent from 200 meters down to 10 meters, with a linear ramp down in descent velocity to 1 m/s. A final descent phase is performed at a constant velocity of 1 m/s until touchdown.

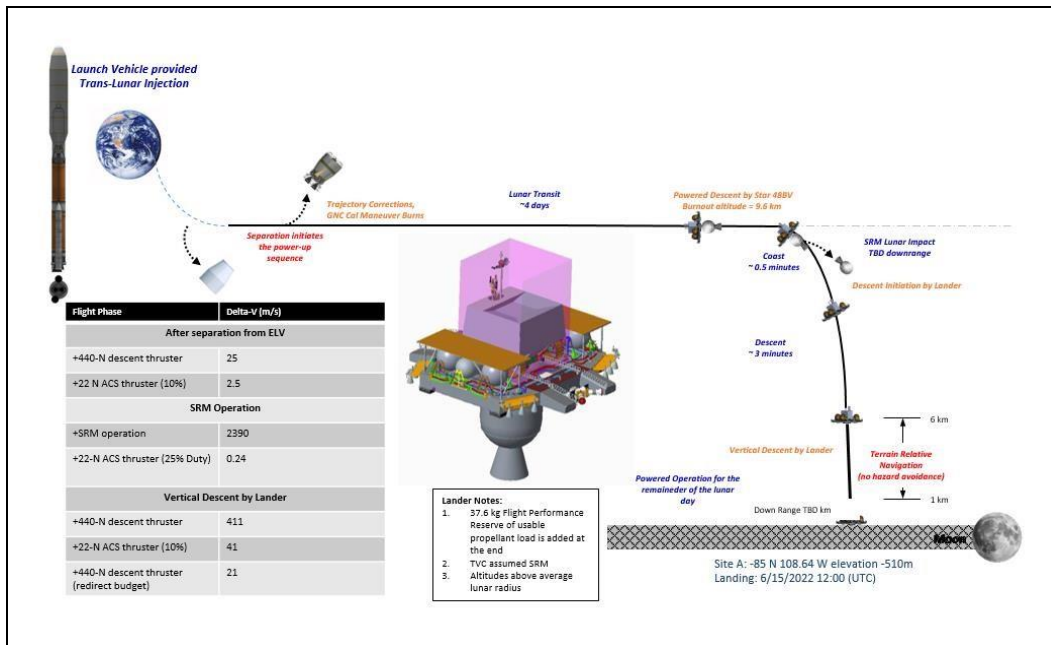


Figure 2. Lunar Pallet Lander Mission Summary.

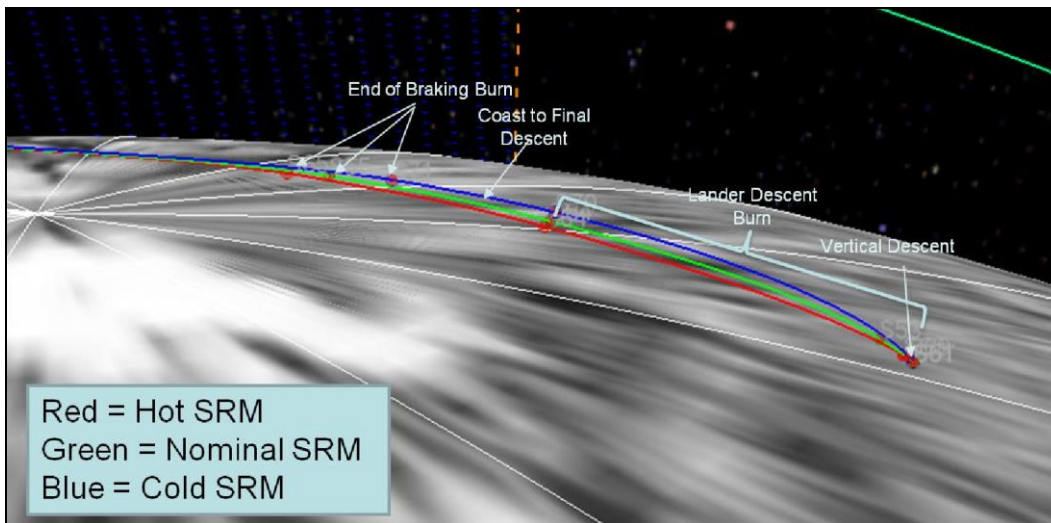


Figure 3. Lunar Pallet Lander Final Descent with SRM Temperature Dispersions

GUIDANCE, NAVIGATION AND CONTROL

GUIDANCE

The Guidance system’s function is to command attitude, angular rates and engine thrust (applicable only to the liquid engines) so that the guidance targets are achieved without violating design constraints. The Guidance system depends on navigated inertial position, inertial velocity, attitude, and the current time from the Navigation subsystem. The Mission Manager supplies the Guidance system with inputs for event notifications and engine status. The remaining inputs to the Guidance algorithms are mission-dependent data and constants, which are loaded onto LPL in the form of loadable parameters. Outputs from the Guidance system passed to the Control system include the estimate of liquid propellant remaining, as well as commanded attitude and angular velocity. Additionally, the Guidance system outputs the recommended shutdown command to the DCS engines. Another study¹⁴ provides a detailed summary of Powered Descent Algorithms.

The Guidance system is divided into four main areas: Coast Guidance, Braking Guidance, Powered Descent Guidance, and Vertical Descent Guidance. Coast Guidance is firstly used in the Pre-SRM mission phase, which starts at the time of separation from the ELV upper stage and ends at the beginning of Solid Rocket Motor (SRM) ignition. There are also two Post-SRM Coast Guidance phases: one between SRM shutdown and ignition of the DCS engines, and one right before the Vertical Decent phase. Braking Guidance occurs during the SRM burn. Powered Descent Guidance, using pulsed liquid engines, occurs after the Post-SRM Coast and lasts until the LPL has achieved a specified target above the landing site. Lastly, the Vertical Descent phase begins at the specified target above the lunar surface and lasts until the LPL touches down at the target site. During each phase, an appropriate guidance scheme is used, with some phases containing multiple guidance schemes to be used for trade studies. Table 1 lists the current choices of guidance algorithms to be used through each phase.

Table 1: Guidance Algorithms by Phase

Phase of Flight	Guidance Routine Option
Pre-SRM Coast	LVLH Hold – adjusts attitude to pre-determined LVLH pitch angle
	MEDeA – runs MEDeA descent algorithm, predicts starting LVLH pitch angle
SRM Burn	LVLH Hold – holds pre-determined LVLH pitch angle through duration of burn
	MEDeA – closed-loop SRM guidance for adjusting commanded LVLH pitch
Post-SRM Coast	Fixed time coast
Powered Decent	An Optimal Guidance Law for Planetary Landing ⁶
	Augmented Apollo Powered Decent Guidance ¹⁶
Vertical Alignment	Optional mode to pitch vehicle vertically
Vertical Decent	Linear velocity ramp-down, then linear position-velocity controller logic

In the Pre-SRM Coast phase, either a fixed known pitch angle relative to Local Vertical Local Horizontal (LVLH) frame is commanded, or a predicted required attitude at the start of the SRM burn is calculated and commanded by running the Moon Entry Descent Algorithm (MEDeA). The MEDeA, a predictor-corrector algorithm for the SRM burn developed by Ellen M. Braden NASA-JSC, is an integrated closed-loop guidance algorithm that accounts for the variations in the SRM thrust profile while staying within the liquid propellant budget. The SRM's thrust profile is estimated using curve fits of the projected hot, cold, and nominal temperature thrust profiles and an on-board calculated burn time. Using this estimated thrust profile, the SRM's pitch angle is adjusted during the descent using a numeric predictor-corrector method to achieve a pre-determined distance from the desired landing site. At the end of the SRM burn and SRM disposal, a second predictor-corrector determines the minimum coast time needed for the vehicle to reach the desired landing site within the liquid propellant budget. The liquid thruster guidance is chosen by the trajectory designer to steer out state errors from the SRM burn and meet the mission constraints. For example, either a minimum acceleration guidance or the Apollo guidance could be used for the liquid powered descent portion.

No guidance attitude is commanded in the Post-SRM Coast phase, and the vehicle is allowed to coast freely either using a fixed time or a time calculated by MEDeA. After the Post-SRM Coast, the liquid Powered Descent phase starts. In the Powered Descent phase, two analytical algorithms are chosen. The first algorithm, developed by D'Souza⁶, is an optimal closed-loop feedback law which was analytically derived using the Euler-Lagrange equations, and assumes a linear acceleration profile. The second algorithm, Augmented Apollo Powered Descent Guidance (A2PDG¹⁶), is also analytical and allows for a wider range of acceleration and trajectory profiles.

An Optimal Guidance Law for Planetary Landing (D'Souza⁶), starts with Euler-Lagrange theory and solves an analytical expression for optimal control. The Cost index function is defined to minimize J given by following equation

$$J = Tt_f + \frac{1}{2} \int (a_x^2 + a_y^2 + a_z^2)$$

Which is subjected to:

$$\begin{aligned} \dot{\vec{r}} &= \vec{v} \\ \dot{\vec{v}} &= \vec{a} - \vec{g}. \end{aligned}$$

Where T is a constant gain and t_f is the final time. a_x, a_y, a_z are components of acceleration expressed in the landing site frame. \vec{r} and \vec{v} are position and velocity, respectively. For the above problem, the flat earth assumption is applicable and \vec{g} is constant. If the objective is to target a final state \vec{r}_f and \vec{v}_f , a linear form of analytical control is found given by following equation:

$$\vec{a} = -\frac{4}{t_{go}} \vec{v} - \frac{6}{t_{go}^2} \vec{r} - \vec{g}$$

In the above equation, t_{go} is the difference between current and the final time. t_{go} can be found by solving the following quartic equation, as referenced in D'Souza:

$$\left(T + \frac{g_z^2}{2}\right) t_{go}^4 - 2\vec{v} \cdot \vec{v} t_{go}^2 - 12\vec{v} \cdot \vec{r} - t_{go} - 18\vec{r} \cdot \vec{r} = 0$$

A2PDG, developed by Ping Lu¹⁶, assumes that the acceleration over the course of the burn takes the form of a quadratic, which is not necessarily optimal but adds an additional degree of control and is near optimal. For example, with D'Souza, a linear form of control allows control of the final position and final velocity. However, a quadratic form of control enables the control of the final acceleration as well. This feature is useful to control the orientation of the lander at the end of the Powered Descent phase. If the

acceleration vector is constrained to align vertically to the landing site, then there is no need for a vertical alignment phase at the end of Powered Descent flight. Ping Lu presents A2PDG in his paper and gives an analytical closed-loop form for thrust direction and magnitude as follows:

$$a_r = \frac{2}{t_{go}} \left(1 - \frac{1}{3} k_r \right) [\vec{v}_f - \vec{v}] + \frac{k_r}{t_{go}^2} [\vec{r}_f - \vec{r} - \vec{v} t_{go}] + \left(\frac{1}{6} k_r - 1 \right) \vec{a}_f + \left(\frac{1}{6} k_r - 2 \right) \vec{g}$$

The A2PDG is chosen as a baseline guidance algorithm for results presented in subsequent sections of this paper.

NAVIGATION

The lander requires highly accurate knowledge of the vehicle’s state during the entire descent mission in order for the closed-loop guidance to achieve the 100m precision landing requirement. The guidance algorithm outlined above is highly susceptible to navigation errors, and small uncertainties in the knowledge of position and velocity will decrease landing accuracy. In order to meet the landing requirements, a robust set of sensors is required to support inertial navigation during descent. A baseline sensor suite, outlined in the next section, was selected to reduce navigation errors taking into account weight and cost, consistent with a NASA class-D mission type.

Baseline Sensor Suite

The integrated sensor package includes a variety of sensors enabling high accuracy knowledge of position and velocity during the descent. At the heart of the navigation system is an inertial measurement unit, with requirements on par with the LN200S³. This IMU was chosen due to the team’s prior experience with the unit on multiple terrestrial platforms¹⁴ and its balance of SWAP, cost, and performance. While this sensor is capable enough to adequately support controls requirements in terms of rate and acceleration knowledge, the uncertainties from pure integration navigation are beyond the landing requirements. Therefore, additional sensors are used to augment the raw inertial measurements. An overview of the sensor suite is provided in Table 2. This suite is used to provide measurements of position and velocity to reduce knowledge errors. The primary aiding source to reduce state errors come from the use of TRN. While this technology has been operational flown on terrestrial vehicles¹¹ and is in development to support future Mars Missions^{12,13,14}, this will be one of the first operational applications of this technology in an extraplanetary landing mission. TRN operates by comparing an in-flight image of the planetary surface to a preloaded map. Using computer vision algorithms, the sensor is able to provide an estimate of a planetrelative position. This accuracy is limited by the fidelity of the onboard map, processing capability, and imaging and lighting characteristics. At this stage of vehicle design, the project is focusing on position measurement accuracy requirements to define the TRN subsystem.

Table 2: Navigation Sensor Suite

Sensor	Measurement	Operational Constraints

³ <https://www.northropgrumman.com/Capabilities/LN200FOG/Documents/ln200s.pdf>

LN200S	High Rate Inertial Acceleration and Angular Rate	Entire Mission
Terrain Relative Navigation	Low Rate Inertial Position	Max Altitude and Min Altitude Constraints
Navigation Doppler LIDAR	High Accuracy 3-D Ranging and Velocity Relative to Surface	4000m to 30m
Star Tracker	Inertial Attitude Measurements	Cruise, up to SRM
Deep Space Network (DSN) Update	Time, Inertial Position and Velocity	Cruise, prior to SRM

While this system does vastly improve translational position knowledge, it does have a limitation in the vertical axis and is coupled with the inherent instability in the vertical axis due to the effect of gravity errors. To provide additional knowledge in the vertical axis and provide a direct velocity measurement to the sensor integration suite, the use of NDL¹⁴ has been baselined. This system provides a high accuracy measurement of both altitude and velocity via the use of multiple laser tracking heads.

One of the primary drivers of the landing performance is the initial uncertainty in terms of position, velocity, and attitude. Additional onboard systems help to limit the initial errors prior to descent. The landing vehicle utilizes a star tracker to maintain a high accuracy attitude solution. This sensor will be used during the initial descent to constrain attitude errors. Similarly, the vehicle utilizes the Deep Space Network to provide a time, position, and velocity update prior to entering the descent maneuvers. Figure 4 defines the sensor data flow and navigation architecture.

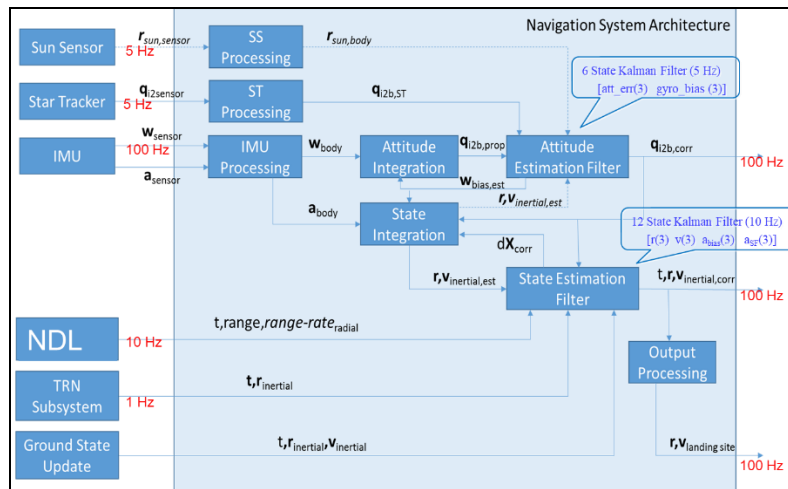


Figure 4. Navigation Architecture

In order to perform system estimation, the individual sensors are all modeled within the six Degrees Of Freedom (6-DOF) simulation framework. This framework utilizes error models specific to each sensor to capture the primary sensitivities. For the inertial navigation sensor, baseline errors such as bias, scale factor, noise, random walk, inter-sensor misalignments, and non-orthogonalities are captured. The star tracker error model has heritage to previous programs utilizing similar hardware modeling attitude error independently about sensor roll and pitch-yaw axes. The TRN system is currently modeled as a sensor providing an inertial state estimate with errors captured in terms of position accuracy. The NDL altimeter

is modeled as lunar-centric velocity and altitude with errors focused on measurement precision, uncertainty, and mounting misalignment. This is necessary to capture the effect of attitude error coupling through the rotation of body-frame measurements into the inertial frame for use in the navigation algorithms. Modeling these errors within this framework allows for both covariance and statistical Monte Carlo-based analysis of the navigation system capabilities. This analysis capable also enables understanding of system sensitivities and requirements developments.

CONTROL

Solid Rocket Motor Control

The SRM utilizes thrust vector control for pitch and yaw, while the roll (roll axis aligned with the SRM thrust direction) control is achieved with the ACS, 5 lbf pulsed thruster control. The SRM control utilizes a classical Proportional Integral Derivative (PID) control algorithm. Figure 5 shows the SRM control response performance for a test condition. The control test corresponds to an initial nozzle angle, β_0 , of 0.5 deg, and SRM lateral thrust misalignment, δ_E , of 1 mm and with a lander center of gravity, c.g., offset of 1 mm. Arbitrary disturbances are also introduced to test the control system at approximately 12 seconds and 20 seconds. Figure 5 shows how the SRM control system rejects the disturbances and aligns the thrust vector angle, Beta, through the center of gravity of the lander, bringing the control error, Pitch error, to zero.

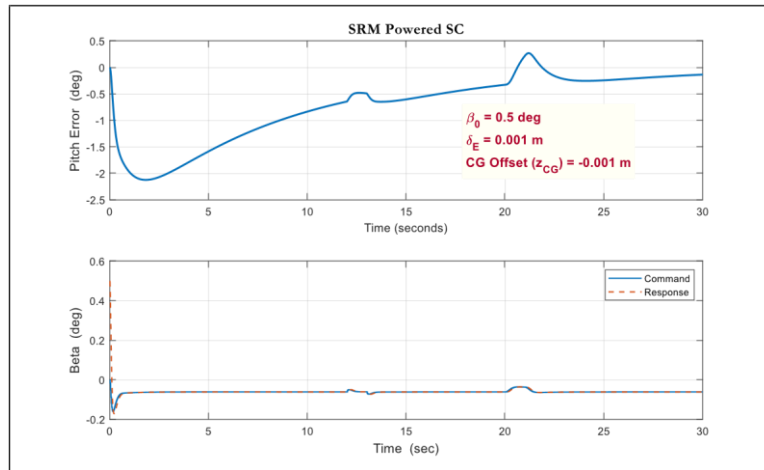


Figure 5. SRM Control Response to Simulated Disturbances

Powered Descent

When using the twelve 100 lbf liquid Descent Engines (DE), the ACS provides control using a phase plane algorithm.¹⁰ The phase-plane, shown in Figure 6, is augmented using Off-Pulsing of the main engines for increased control authority. Off-Pulsing, which is to purposely turn off selected engines pairs to generate a torque on the vehicle, provides larger control authority than the 5 lbf ACS thrusters. Large control authority may be needed if there is a large, > 1 cm, offset in the lander center of gravity with respect to the vehicle centerline, generating a large torque during powered descent that could easily overpower the 5 lbf ACS system. Large or unexpected center of gravity shifts could be caused by a non-uniform draining of fuel and oxidizer tanks on each side of the vehicle, a phenomenon called differential draining. Figure 6, shows that for small rate errors, $d\theta/dt$, and angle errors, θ , region in between the blue lines, the control system will not fire the 5 lbf thrusters. However, attitude and attitude rate error combinations higher than the blue lines but up to the first red dashed line, the ACS takes control and fires the 5 lbf thrusters to reject the disturbance. Once the rate and/or the angle errors become large such that they exceed the 5ms red-dash line, then an Off-

Pulse of 5ms, that is shutting a selected pair of engines for 5 ms, will be applied to produce a counter torque to reduce the control error. Similarly, if the rate and angle attitude errors exceed the 10ms dashed line or even 20ms, an Off-Pulse of the 10ms and 20ms will be applied, respectively.

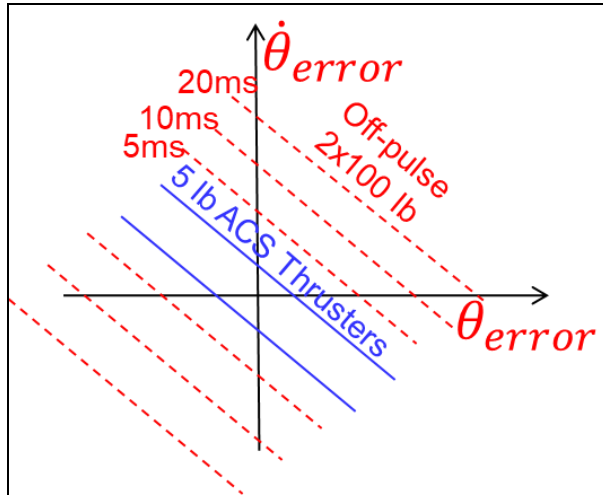


Figure 6. Liquid Engine Phase-Plane Control

Using the above phase plane, the power descent control error is shown below in Figure 7. During liquid power descent, “Optimal Descent” and “Vertical” flight phases in Figure 7, the control angle error is kept within approximately 1 deg, (b), and about 2 deg/sec for angle rate, (c), where X, Y, Z correspond to roll, pitch, yaw, and roll axis is co-axial with thrust the vector.

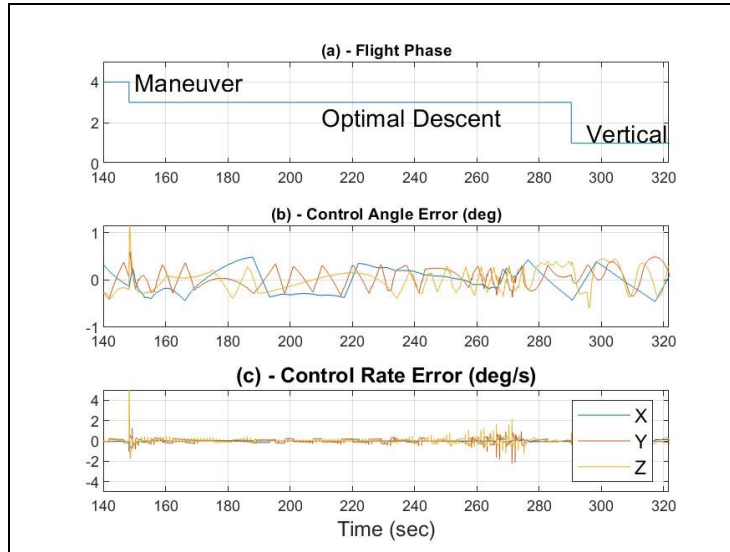


Figure 7. (a) Flight Phase, (b) Control Angle Error, (c) Control Rate Error

GENERALIZED LANDER SIMULATION TOOL

The Generalized LAnder Simulation in Simulink (GLASS) tool was created to be a modular, userfriendly, and capable of performing multi-body 6-DOF simulation. The primary advantage of GLASS is that allows the user to generate code in the friendly Simulink environment while having the capability of automatically generating flight code in “C” language. In addition, GLASS leverages many tools and features available in the Mathworks Simulink environment, such as the Control Design toolbox for control development and tuning and the Simulink Test, and Simulink Coverage for unit testing of the GNC code, just to name a few. GLASS is built using the latest version of Matlab/Simulink (2018a) in order to take advantage of the newest features and improvements of the software.

While GLASS is currently being utilized for the simulation of landers, it is capable of simulating a variety of spacecraft. The core dynamics engine of the simulation can be easily modified to model a new craft. Figure 8, shows the main breakdown of a generic spacecraft modeling in GLASS. Plant corresponds to the lander applied forces and torques typically propulsion and gravity models, while the core dynamics corresponds to modeling of the lander Newtonian mechanics, using the Matlab Simscape Multibody 6-DOF simulation engine. The Matlab Simscape simulation engine can be applied to any vehicle: landers, ascent stages, satellites, rovers, etc. Figure 9, shows how all forces and torques are computed separately and applied to the 6-DOF multi-body Simscape dynamic core. This also allows GLASS to model multiple spacecraft within the same simulation environment.

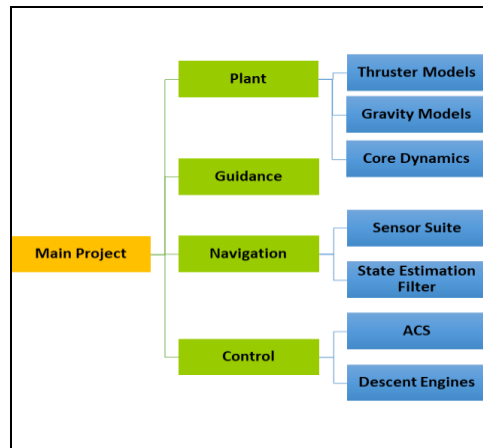


Figure 8. Six degrees of freedom GLASS tool architecture and models

GLASS is capable of simulating landers in a variety of environments. The current possible environments include a flat or spherical-planet mode, and Earth-Moon and Sun-Earth-Moon systems. These modes allow the user to choose a level of fidelity appropriate to the design cycle. The Earth-Moon and Sun-EarthMoon systems utilize the NASA Jet Propulsion Laboratory’s (JPL) SPICE toolkit to calculate the planetary-ephemeris data, used by GLASS to drive the positions of the celestial bodies. While currently only combinations of the Sun, Earth, and Moon are modeled, other planetary bodies can be modeled as well.

GLASS is also capable of running different gravity models depending on the desired level of fidelity required. The standard gravity model in GLASS is a pure spherical gravity model; however, the user may also select a spherical harmonic gravity model.

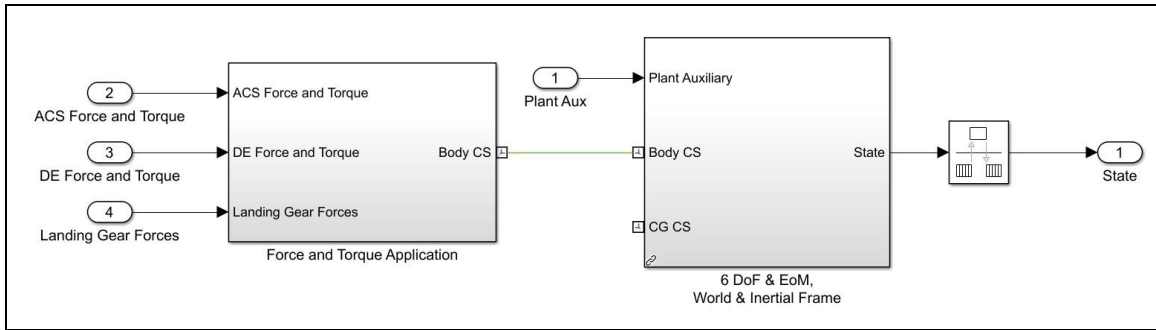


Figure 9. GLASS tool snapshot showing vehicle forces and torques applied to 6-DOF multi-body dynamics core.

LANDER PERFORMANCE

Event Timeline

Before SRM ignition, DSN will be used to determine and upload the vehicle’s navigation state (time, velocity and position) and an SRM ignition time. Figure 10 shows the altitude timeline, with SRM ignition starting at about 75 km above the lunar surface. SRM reduces most of the orbital tangential velocity, with a burnout occurring at about 10 km above the lunar surface. After SRM burnout, a short coast period is used to re-orient the vehicle for optimal liquid power descent. The coast time is also used to turn on the TRN sensor without any propulsion dynamics, vibrations and plume, to increase the chances of a good lunar surface image that can provide the first update the vehicle’s position with respect to the lunar surface. Then, at approximately 7.8 km above the surface, the liquid engines fire initiating powered descent, lasting all the way until engine-shutdown, a few meters above the surface. At about 2 km above the lunar surface, the NDL sensor is turned on, providing altitude and velocity state updates until about 30 meters above the surface. From previous Apollo missions, it has been observed that at about 30 meters, the descent engines may start kicking up lunar dust, and NDL measurements may not be reliable on a dusty environment; however further work is needed to refine NDL cutoff altitude. Finally, it is assumed that TRN will stop providing position estimates at approximately 500 m above the surface, since TRN lunar surface maps may not have enough resolution to determine position, but future work will determine precise TRN cut-off altitude.

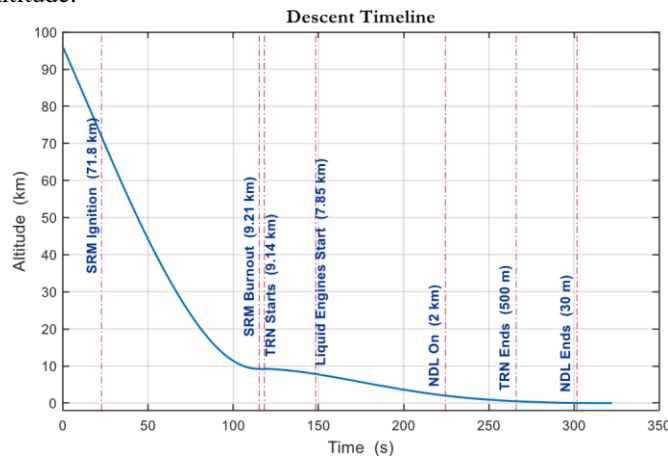


Figure 10. Event and Sensor Altitude Timeline

Performance Results

The lander performance was evaluated conducting a 200-case Monte Carlo analysis with dispersions that include mass properties, navigation sensor noise parameters, and propulsion performance parameters. Figure 11-left, shows the dispersed altitude vs. time, while Figure 11-right, shows touchdown positions relative to the landing target. Landing precision is well below the required 100-meter precision, mostly due to the combination of TRN and NDL. Without TRN, landing position precision is expected to be in the order of kilometers, typical of historic lunar and planetary missions.

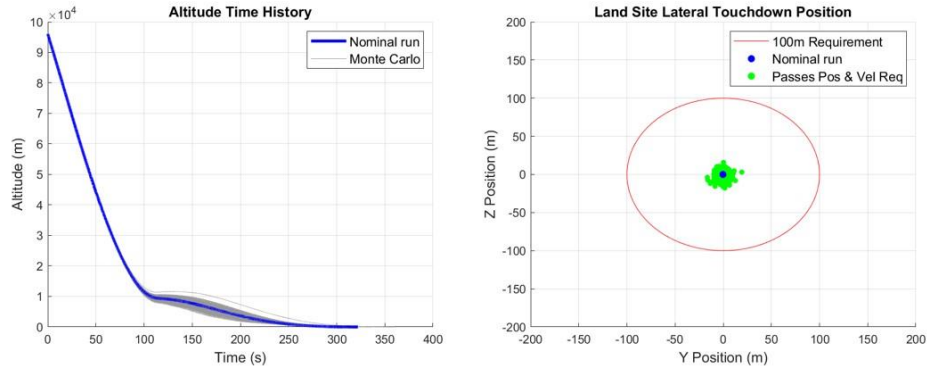


Figure 11. Altitude profile and Landing Precision.

In addition, landing velocities are also assessed with dispersed analysis, critical for achieving a “soft” touchdown. Figure 12 shows the dispersed touchdown velocities. Vertical touchdown velocities stay below approximately 1.5 m/s, and below the required 2 m/s. Similarly, lateral velocities stay below the required 2 m/s to avoid lander tip-over.

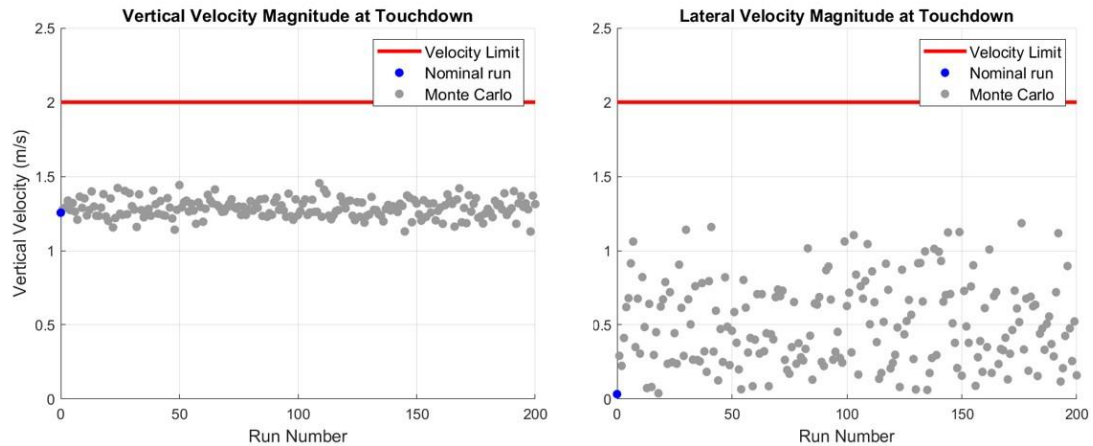


Figure 12. Touchdown Velocity.

Finally, propellant remaining at touchdown is tracked in Figure 13. Most of the cases show at least approximately 40 kg of unburned propellant; however, a single case shows a low propellant margin of about 15 kg. This low propellant margin outlier corresponds to a large dispersed center of gravity offset case, which causes the SRM to finish its breaking burn at a higher altitude; and thus, more propellant is used to bring the

lander to the surface. To avoid this kind of outliers, future work includes implementation of a guidance correction algorithm.

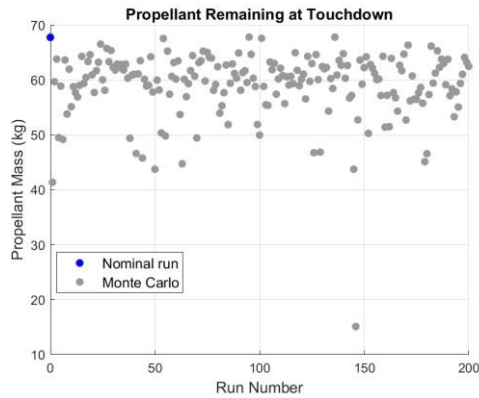


Figure 13. Remaining Propellant at Touchdown.

SUMMARY AND FUTURE WORK

This paper provides a summary of the guidance, navigation, control, and mission design for the Lunar Pallet Lander. In addition, the paper shows preliminary dispersed Monte Carlo analysis demonstrating that the lander meets the mission precision landing and touchdown velocity requirements. However, to meet the mission requirements, the LPL must have accurate position knowledge during descent, which can only be achieved with TRN, currently at different stages of development, and with its first inspace application planned for the NASA-JPL Mars 2020 mission. Furthermore, to meet the touchdown velocity requirements, accurate velocity measurements are needed, which are achieved through use of the NASA-NDL sensor, currently under development, with expected in-space flight opportunities in the next 2-3 years. This paper discusses advances in the development of high fidelity lander simulations tool, GLASS, which allows in-depth analysis and trade studies on sensors, propulsion, and GNC algorithms. The high fidelity lander simulation tool allows us to explore the complex interactions between navigation sensors, guidance algorithm, propulsion systems, etc. to bound trade spaces, develop key lander requirements, and perform sensor selection. Future work includes increasing lander modeling fidelity, including flexible body and slosh dynamics, further refinement of GNC algorithms, and incorporation of sensor alignment uncertainties, and accurate sensor cut-off altitudes. Finally, the advance of a lander design with precision, autonomous, and soft landing capabilities lays the foundation for future human missions.

ACKNOWLEDGMENTS

The team would like to acknowledge the support of the Lunar Pallet Lander project in supporting this work and publication. Additionally, we would like to express our gratitude for the support of our branch and division management in their continued support of small project and technology development missions.

REFERENCES

- ¹ Olansen, J., Munday.S., Mitchell, J., "Project Morpheus: Lessons Learned in Lander Technology Development", AIAA Space 2013 Conference, Sept. 2013, San Diego, CA.
- ² S. Craig, J. P. Holt, M. R. Hannan, and J. I. Orphee, "Mission Design for the Lunar Pallet Lander," AAS/AIAA Space Flight Mechanics Meeting, January 2019. AAS 19-330.

- ³ J.-W. Jang, S. Bhatt, M. Fritz, D. Woffinden, D. May, E. Braden, and M. Hannan, "Linear Covariance Analysis for a Lunar Lander," AIAA Guidance, Navigation, and Control Conference, AIAA SciTech Forum, 2017. AIAA-20171499.
- ⁴ Klumpp, Allan R., "Apollo Lunar-Descent Guidance", Charles Stark Draper Laboratory, R-695, June 1971. ⁵ D. Pierrottet, F. Amzajerdian, L. Petway, B. Barnes, G. Lockard, G. Hines, "Navigation Doppler lidar sensor for precision altitude and vector velocity measurements: flight test results", Proc. SPIE 8044, Sensors and Systems for Space Applications IV, 80440S (23 May 2011)
- ⁶ D'Souza, Christopher, "An Optimal Guidance Law for Planetary Landing", AIAA-97_3709, 1997
- ⁷ Crassidis, John and Junkins, John, "Orbital Estimation of Dynamic Systems", Second Edition, CRC Press, 2012. ⁸ E. Anzalone, E. Braden, N. Ahmad, D., K. Miller, "Guidance and Navigation Design Trades for the Lunar Pallet Lander" 42nd Annual American Astronautical Society Guidance and Control Conference; Feb 1 – Feb 6 2011; Breckenridge, Colorado, AAS 19-091.
- ⁹ McGee, T., Kaidy, J., Reid, D., Oxtan, G., "Guidance, Navigation, and Control Development for A Robotic Lander Testbed," 33rd Annual American Astronautical Society Guidance and Control Conference; Feb 5 – Feb 9 2011; Breckenridge, Colorado, AAS 11-032.
- ¹⁰ Hall, R. Hough, S., Orphee, C., Clemens, K., "Design and Stability of an On-Orbit Attitude Control System Using Reaction Control Thrusters," AIAA Guidance, Navigation, and Control Conference, 2016, pp. 0087.
- ¹¹ Pierrottet, Diego, et al. "Navigation Doppler Lidar sensor for precision altitude and vector velocity measurements: flight test results." Sensors and Systems for Space Applications IV. Vol. 8044. International Society for Optics and Photonics, 2011.
- ¹² Johnson, Andrew E., and James F. Montgomery. "Overview of terrain relative navigation approaches for precise lunar landing." 2008 IEEE Aerospace Conference. IEEE, 2008.
- ¹³ Johnson, Andrew E., et al. "Design and analysis of map relative localization for access to hazardous landing sites on mars." AIAA Guidance, Navigation, and Control Conference. 2016.
- ¹⁴ Johnson, Andrew E., et al. "Real-time terrain relative navigation test results from a relevant environment for Mars landing." AIAA Guidance, Navigation, and Control Conference. 2015.
- ¹⁵ Ronald Sostaric and Jeremy Rea. "Powered Descent Guidance Methods For The Moon and Mars", AIAA Guidance, Navigation, and Control Conference and Exhibit, Guidance, Navigation, and Control and Co-located Conferences, 2005.
- ¹⁶ Lu, Ping. "Augmented Apollo Powered Descent Guidance." Journal of Guidance, Control, and Dynamics, AIAA, 2018.